PHYSICAL REVIEW D VOLUME 51, NUMBER 6 15 MARCH 1995

Chiral symmetry breaking in quenched massive strong-coupling four-dimensional QED

Frederick T. Hawes
Department of Physics and SCRI, Florida State University, Tallahassee, Florida 32306-3016

Anthony G. Williams
Department of Physics and Mathematical Physics, University of Adelaide, South Australia 5005, Australia
(Received 14 October 1994)

We present results from a study of subtractive renormalization of the fermion propagator Dyson-Schwinger equation (DSE) in massive strong-coupling quenched four-dimensional QED. The results are compared for three different fermion-photon proper vertex *Ansätze*: bare γ^μ, minimal Ball-Chiu, and Curtis-Pennington *Ansätze*. The procedure is straightforward to implement and numerically stable. This is the first study in which this technique is used and it should prove useful in future DSE studies, whenever renormalization is required in numerical work.

PACS number(s): 11.30.Rd, 11.30.Qc, 12.20.Ds

I. INTRODUCTION

Strong-coupling QED in three space and one time dimension has been studied within the Dyson-Schwinger equation (DSE) formalism for some time [1–3], in order to see whether there may be a phase transition to a nontrivial "local" theory at high momenta [2,4–6], as a model for dynamical chiral-symmetry-breaking (DCSB) in walking technicolor theories [7,8], and also as an abelianized model for nonperturbative phenomena in QCD [9,10]. For a recent review of Dyson-Schwinger equations and their application see Ref. [11]. The usual approach is to write the DSE for the fermion propagator or self-energy, possibly including equations for the photon vacuum polarization [12,13] or the fermion-photon proper vertex [1]. An *Ansatz* is made for the undefined Green's functions that contain the infinite continuation of the tower of DSE's. The resulting nonlinear integral equations are solved numerically in Euclidean space [14] by iteration. DCSB occurs when the fermion propagator develops a nonzero scalar self-energy in the absence of an explicit chiral-symmetry-breaking (ECSB) fermion mass. We refer to coupling constants strong enough to induce DCSB as supercritical and those weaker are called subcritical. We write the fermion propagator as

$$S(p) = \frac{Z(p^2)}{\not{p} - M(p^2)} = \frac{1}{A(p^2)\,\not{p} - B(p^2)}\ , \qquad (1)$$

with $Z(p^2)$ the finite momentum-dependent fermion renormalization, and $B(p^2)$ the scalar self-energy. In the massless theory (i.e., in the absence of an ECSB bare electron mass) by definition DCSB occurs when $B(p^2) \neq 0$. Note that $A(p^2) \equiv 1/Z(p^2)$ and $M(p^2) \equiv B(p^2)/A(p^2)$.

Many studies, even until quite recently, have used the bare vertex as an *Ansatz* for the one-particle irreducible (1PI) vertex $\Gamma^\nu(k,p)$ [2,4,5,8,9,12,13,15], despite the fact that this violates the Ward-Takahashi identity (WTI) [16]. It is also common, especially in studies motivated by walking technicolor theories [7], to find vertex *Ansätze* which claim to solve the WTI, but which still possess kinematic singularities in the limit of zero photon momentum $q^2 = (k-p)^2 \to 0$ [17,18]. With any of these *Ansätze*, the resulting fermion propagator is not gauge covariant, i.e., physical quantities such as the critical coupling for dynamical symmetry breaking, or the mass itself, are gauge dependent [17]. A general form for $\Gamma^\nu(k,p)$ which does satisfy the Ward identity was given by Ball and Chiu in 1980 [19]; it consists of a minimal longitudinally constrained term which satisfies the WTI, and a set of tensors spanning the subspace transverse to the photon momentum q.

Although the WTI is necessary for gauge invariance, it is not a sufficient condition; further, with many of these vertex *Ansätze* the fermion propagator DSE is not multiplicatively renormalizable, which is equivalent to saying that overlapping logarithms are present. There has been much recent research on the use of the transverse parts of the vertex to ensure both gauge covariant and multiplicatively renormalizable solutions [20–28], some of which will be discussed below.

What is common to essentially all of the studies so far is that the fermion propagator is not in practice subtractively renormalized. Most of these studies have assumed an initially massless theory and have renormalized at the ultraviolet cutoff of the integrations, taking $Z_1 = Z_2 = 1$. Where a nonzero bare mass has been used [6,12], it has simply been added to the scalar term in the propagator. Although there have been formal discussions of the renormalization [5,6,23,26], the important step of subtractive renormalization has not been performed.

We describe here the results of a study of subtractive renormalization in the fermion DSE, in quenched strong-coupling four-dimensional QED (QED_4). (In the context of this study of QED, the term "quenched" means that the bare photon propagator is used in the fermion self-energy DSE, so that $Z_3 = 1$. Virtual fermion loops may still be present, however, within the vertex corrections.) We believe this is the first calculation in which the subtraction is performed numerically as the inte-

gral equations are being iterated. This new technique should prove useful in other DSE studies. Results are obtained for DSE with three different vertices: the bare γ^μ, the minimal Ball-Chiu vertex form [19], and the Curtis-Pennington vertex [23–26].

Organization of the paper is as follows. The DSE for the renormalized fermion propagator, and *Ansätze* for the proper vertex, are discussed in Sec. II. The subtractive renormalization is described in Sec. III. Section IV A presents results at subcritical couplings, while Sec. IV B discusses the results for couplings above the DCSB threshold. Conclusions and discussion are given in Sec. V.

II. DSE AND VERTEX ANSÄTZE

The DSE for the renormalized fermion propagator, in a general covariant gauge, is

$$S^{-1}(p^2) = Z_2(\mu,\Lambda)[\not{p} - m_0(\Lambda)] - iZ_1(\mu,\Lambda)e^2\int^\Lambda \frac{d^4k}{(2\pi)^4}\gamma^\mu S(k)\Gamma^\nu(k,p)D_{\mu\nu}(q)\,; \tag{2}$$

here $q = k - p$ is the photon momentum, μ is the renormalization point, and Λ is a regularizing parameter (taken here to be an ultraviolet momentum cutoff). We write $m_0(\Lambda)$ for the regularization-parameter dependent bare mass. In the massless theory (i.e., in the absence of an ECSB) the bare mass is zero, $m_0(\Lambda) = 0$. The physical charge is e (as opposed to the bare charge e_0), and the general form for the photon propagator is

$$D^{\mu\nu}(q) = \left\{\left(-g^{\mu\nu} + \frac{q^\mu q^\nu}{q^2}\right)\frac{1}{1-\Pi(q^2)} - \xi\frac{q^\mu q^\nu}{q^2}\right\}\,, \tag{3}$$

with ξ the covariant gauge parameter. Since we will work in the quenched approximation and the Landau gauge we have $e^2 \equiv e_0^2 = 4\pi\alpha_0$ and

$$D^{\mu\nu}(q) \to D_0^{\mu\nu}(q) = \left(-g^{\mu\nu} + \frac{q^\mu q^\nu}{q^2}\right)\frac{1}{q^2}\,, \tag{4}$$

for the photon propagator.

A. Vertex Ansatz

The requirement of gauge invariance in QED leads to the Ward-Takahashi identities (WTI); the WTI for the fermion-photon vertex is

$$q_\mu\Gamma^\mu(k,p) = S^{-1}(k) - S^{-1}(p)\,, \tag{5}$$

where $q = k - p$ [29,30]. This is a generalization of the original differential Ward identity, which expresses the effect of inserting a zero-momentum photon vertex into the fermion propagator,

$$\frac{\partial S^{-1}(p)}{\partial p_\nu} = \Gamma^\nu(p,p)\,. \tag{6}$$

In particular, it guarantees the equality of the propagator and vertex renormalization constants, $Z_2 \equiv Z_1$. The Ward-Takahashi identity is easily shown to be satisfied order by order in perturbation theory and can also be derived nonperturbatively.

As discussed in [11,31], this can be thought of as just one of a set of six general requirements on the vertex: (i) the vertex must satisfy the WTI; (ii) it should contain no kinematic singularities; (iii) it should transform under charge conjugation (C), parity inversion (P), and time reversal (T) in the same way as the bare vertex, e.g.,

$$C^{-1}\Gamma_\mu(k,p)C = -\Gamma_\mu^T(-p,-k) \tag{7}$$

(where the superscript T indicates the transpose); (iv) it should reduce to the bare vertex in the weak-coupling limit; (v) it should ensure multiplicative renormalizability of the DSE in Eq. (2); and (vi) the transverse part of the vertex should be specified to ensure gauge covariance of the DSE.

Ball and Chiu [19] have given a description of the most general fermion-photon vertex that satisfies the WTI; it consists of a longitudinally constrained (i.e., "Ball-Chiu") part $\Gamma^\mu_{\rm BC}$, which is a minimal solution of the WTI, and a basis set of eight transverse vectors $T_i^\mu(k,p)$, which span the hyperplane specified by $q_\mu T_i^\mu(k,p) = 0$, $q \equiv k - p$. The minimal longitudinally constrained part of the vertex is given by

$$\Gamma^\mu_{\rm BC}(k,p) = \frac{1}{2}[A(k^2)+A(p^2)]\gamma^\mu + \frac{(k+p)^\mu}{k^2-p^2}\left\{[A(k^2) - A(p^2)]\frac{\not{k}+\not{p}}{2} - [B(k^2)-B(p^2)]\right\}. \tag{8}$$

The transverse tensors are given by

$$T_1^\mu(k,p) = p^\mu(k\cdot q) - k^\mu(p\cdot q)\,, \tag{9}$$
$$T_2^\mu(k,p) = (\not{p}+\not{k})T_1^\mu\,, \tag{10}$$
$$T_3^\mu(k,p) = q^2\gamma^\mu - q^\mu\not{q}\,, \tag{11}$$
$$T_4^\mu(k,p) = p^\nu k^\lambda\sigma_{\nu\lambda}T_1^\mu\,, \tag{12}$$
$$T_5^\mu(k,p) = \sigma^{\mu\nu}q_\nu\,, \tag{13}$$
$$T_6^\mu(k,p) = \gamma^\mu(k^2-p^2) - (k+p)^\mu\not{q}\,, \tag{14}$$
$$T_7^\mu(k,p) = \frac{(k^2-p^2)}{2}[\gamma^\mu(\not{p}+\not{k}) - (k+p)^\mu] + (k+p)^\mu p^\nu k^\lambda\sigma_{\nu\lambda}\,, \tag{15}$$
$$T_8^\mu(k,p) = -\gamma^\mu p^\lambda k^\nu\sigma_{\lambda\nu} - p^\mu\not{k} - k^\mu\not{p}\,. \tag{16}$$

A general vertex is then written as

$$\Gamma^\mu(k,p) = \Gamma^\mu_{\rm BC}(k,p) + \sum_{i=1}^{8} \tau_i(k^2,p^2,q^2) T_i^\mu(k,p) , \quad (17)$$

where the τ_i are functions which must be chosen to give the correct C, P, and T invariance properties.

The work of Curtis and Pennington (CP) [23–26] was mentioned above in connection with the specification of the transverse vertex terms in order to produce gauge invariant and multiplicatively renormalizable solutions to the DSE. In the framework of massless QED_4, they eliminate four of the transverse vectors since they are Dirac even and must generate a scalar term. By requiring that the vertex $\Gamma^\mu(k,p)$ reduce to the leading log result for $k \gg p$ they are led to eliminate all the transverse basis vectors except T_6^μ, with a dynamic coefficient chosen to make the DSE multiplicatively renormalizable. This coefficient has the form

$$\tau_6(k^2,p^2,q^2) = \frac{1}{2}[A(k^2) - A(p^2)]/d(k,p) , \quad (18)$$

where $d(k,p)$ is a symmetric, singularity-free function of k and p, with the limiting behavior $\lim_{k^2 \gg p^2} d(k,p) = k^2$. [Here, $A(p^2) \equiv 1/Z(p^2)$ is their $1/\mathcal{F}(p^2)$.] For purely massless QED, they find a suitable form, $d(k,p) = (k^2 - p^2)^2/(k^2 + p^2)$. This is generalized to the case with a dynamical mass $M(p^2)$, to give

$$d(k,p) = \frac{(k^2-p^2)^2 + [M^2(k^2) + M^2(p^2)]^2}{k^2+p^2} . \quad (19)$$

They establish that multiplicative renormalizability is retained up to next-to-leading-log order in the DCSB case. Subsequent papers establish the form of the solutions for the renormalization and the mass [25] and studied the gauge dependence of the solutions [26]. Dong, Munczek, and Roberts [27] subsequently showed that the lack of exact gauge covariance of the solutions was due to the use of a hard cutoff in the integral equations. The fact that there is still some residual gauge dependence in the physical observables such as the chiral critical point shows that with a hard cutoff the CP vertex *Ansatz* is not yet the ideal choice. Dong, Munczek, and Roberts [27] derived an *Ansatz* for the transverse vertex terms which satisfies the WTI and makes the fermion propagator gauge covariant.

Bashir and Pennington [28] have recently described a vertex *Ansatz* which makes the fermion self-energy exactly gauge covariant, in the sense that the critical point for the chiral phase transition is independent of gauge. Their work is a continuation of that of Dong, Munczek, and Roberts, and indeed their vertex *Ansatz* corresponds to the general form suggested in [27]. However, the kinematic factors $\tau_{2,3,6,8}$ are extremely complicated in form and depend upon a pair of as yet undetermined functions $W_{1,2}(k^2,p^2)$ which must be chosen to guarantee that the weak-coupling limit of Γ^μ matches the perturbative result. Renormalization studies of the DSE using this vertex *Ansatz* should be interesting and represent a direction for further research.

In any case, for the solutions to the fermion DSE using the CP vertex, the critical point for the chiral phase transition has been shown to have a much weaker gauge dependence than that for the DSE with the bare or minimal Ball-Chiu vertices [32]. In this work we will primarily use the Curtis-Pennington *Ansatz* but for the sake of comparison will also present results for the bare vertex. Some solutions are also obtained with the minimal Ball-Chiu vertex which, like the Curtis-Pennington vertex, satisfies the WTI, but which does not lead to approximately gauge-invariant solutions nor multiplicative renormalizability.

For each vertex *Ansatz*, the equations are separated into a Dirac-odd part describing the finite propagator renormalization $A(p^2)$, and a Dirac-even part for the scalar self-energy, by taking $\frac{1}{4}$Tr of the DSE multiplied by $\not{p}/p^2$ and 1, respectively. The equations are solved in Euclidean space and so the volume integrals $\int d^4k$ can be separated into angle integrals and an integral $\int dk^2$; the angle integrations are easy to perform analytically, yielding the two equations which will be solved numerically.

III. THE SUBTRACTIVE RENORMALIZATION

The subtractive renormalization of the fermion propagator DSE proceeds similarly to the one-loop renormalization of the propagator in QED. (This is discussed in [11] and in [33], p. 425ff.) One first determines a finite, *regularized* self-energy, which depends on both a regularization parameter and the renormalization point; then one performs a subtraction at the renormalization point, in order to define the renormalization parameters Z_1, Z_2, Z_3 which give the full (renormalized) theory in terms of the regularized calculation.

A review of the literature of DSEs in QED shows, however, that this step is actually never performed. Curtis and Pennington [26], for example, define their renormalization point at the UV cutoff. Miransky [5] gives a formal discussion of the variation of the mass renormalization $Z_m(\mu,\Lambda)$, but does not implement it numerically.

Many studies take $Z_1 = Z_2 = 1$ [20,22–26]; this is a reasonable approximation in cases where the coupling α_0 is small (i.e., $\alpha_0 \lesssim 1.15$), but if α_0 is chosen large enough, the value of the dynamical mass at the renormalization point may be significantly large compared with its maximum in the infrared. For instance, in [26], figures for the fermion mass are given with $\alpha_0 = 0.97$, 1.00, 1.15, and 2.00 in various gauges. For $\alpha_0 = 2.00$, the fermion mass at the cutoff is down by only an order of magnitude from its limiting value in the infrared.

Repeating the arguments from [11], one defines a regularized self-energy $\Sigma'(\mu,\Lambda;p)$, leading to the DSE for the renormalized fermion propagator:

$$\begin{aligned}\widetilde{S}^{-1}(p) &= Z_2(\mu,\Lambda)[\not{p} - m_0(\Lambda)] - \Sigma'(\mu,\Lambda;p) \\ &= \not{p} - m(\mu) - \widetilde{\Sigma}(\mu;p) , \end{aligned} \quad (20)$$

where the (regularized) self-energy is

$$\Sigma'(\mu,\Lambda;p) = iZ_1(\mu,\Lambda)e^2 \int^{\Lambda} \frac{d^4k}{(2\pi)^4}\gamma^\lambda \widetilde{S}(\mu;k)\widetilde{\Gamma}^\nu(\mu;k,p)\widetilde{D}_{\lambda\nu}(\mu;(p-k)) \,. \tag{21}$$

[To avoid confusion we will follow Ref. [11] and in this section *only* we will denote regularized quantities with a prime and renormalized ones with a tilde, e.g., $\Sigma'(\mu,\Lambda;p)$ is the regularized self-energy depending on both the renormalization point μ and regularization parameter Λ and $\widetilde{\Sigma}(\mu;p)$ is the renormalized self-energy.] As suggested by the notation (i.e., the omission of the Λ dependence) renormalized quantities must become independent of the regularization parameter as the regularization is removed (i.e., as $\Lambda \to \infty$). The self-energies are decomposed into Dirac and scalar parts:

$$\Sigma'(\mu,\Lambda;p) = \Sigma'_d(\mu,\Lambda;p^2)\ \not{p} + \Sigma'_s(\mu,\Lambda;p^2)$$

[and similarly for the renormalized quantity, $\widetilde{\Sigma}(\mu,p)$]. By imposing the renormalization boundary condition

$$\widetilde{S}^{-1}(p)\Big|_{p^2=\mu^2} = \not{p} - m(\mu) \,, \tag{22}$$

one gets the relations

$$\widetilde{\Sigma}_{d,s}(\mu;p^2) = \Sigma'_{d,s}(\mu,\Lambda;p^2) - \Sigma'_{d,s}(\mu,\Lambda;\mu^2) \tag{23}$$

for the self-energy,

$$Z_2(\mu,\Lambda) = 1 + \Sigma'_d(\mu,\Lambda;\mu^2) \tag{24}$$

for the renormalization, and

$$m_0(\Lambda) = \left[m(\mu) - \Sigma'_s(\mu,\Lambda;\mu^2)\right]/Z_2(\mu,\Lambda) \tag{25}$$

for the bare mass. In order to reproduce the case with no ECSB mass, for a given cutoff Λ, one chooses $m(\mu) = \Sigma'_s(\mu,\Lambda;\mu^2)$ so that the bare mass $m_0(\Lambda)$ is zero. The mass renormalization constant is given by

$$Z_m(\mu,\Lambda) = m_0(\Lambda)/m(\mu) \,, \tag{26}$$

i.e., as the ratio of the bare to the renormalized mass.

The vertex renormalization $Z_1(\mu,\Lambda)$ is identical to $Z_2(\mu,\Lambda)$ as long as the vertex *Ansatz* satisfies the Ward identity; this is how it is recovered for multiplication into $\Sigma'(\mu,\Lambda;p)$ in Eq. (21). It will be noticed that this is inappropriate for the bare-vertex *Ansatz* since it fails to satisfy the WTI; nonetheless, since for the bare-vertex case there is no way to determine $Z_1(\mu,\Lambda)$ independently, we will use $Z_1 = Z_2$ for the sake of comparison. In the Landau gauge for the bare vertex these will then both be 1, since in this case $\Sigma'_d(\mu,\Lambda;p^2) = 0$ for all p^2 as is well known [11].

We carry out this step of the renormalization, using the bare vertex γ^μ, the minimal Ball-Chiu vertex of Eq. (8), and that with the Curtis-Pennington transverse term added [see Eqs. (18,19)]. The equations are again first written in Minkowski space, and then rotated to Euclidean space. These are then solved by iteration from an initial guess, with a wide range of cutoffs, and with various renormalization points μ^2 and renormalized masses $m(\mu)$.

IV. RESULTS

Solutions were obtained for the DSE with the Curtis-Pennington and bare vertices, for couplings α_0 from 0.1 to 1.75; solutions were also obtained for the minimal Ball-Chiu vertex, with couplings α_0 from 0.1 to 0.6 (for larger couplings, the DSE with this vertex was susceptible to numerical noise). In Landau gauge, the critical coupling for the DSE with bare vertex is $\alpha_c^{\rm bare} = \pi/3$, the critical coupling for the Curtis-Pennington vertex is $\alpha_c^{\rm CP} = 0.933667$ [32], and that for the Ball-Chiu vertex is expected to be close to these two values. Since there are some qualitative differences between the solutions with subcritical and supercritical couplings, we shall describe these separately.

A. Subcritical couplings

Solutions for the Curtis-Pennington and bare vertex *Ansätze* were obtained for values of the coupling α_0 from 0.1 to 0.9. The program using the Ball-Chiu vertex was also run, with couplings α_0 from 0.1 to 0.6. For the solutions in the subcritical range, the renormalization point $\mu^2 = 100$, and renormalized masses were either $m(\mu) = 10$ or 30. Ultraviolet cutoffs were 1.0×10^{12} and 1.0×10^{18}.

The family of solutions for the Curtis-Pennington vertex with $m(\mu) = 10$ is shown in Fig. 1. Figure 1(a) shows the finite renormalization $A(p^2)$; note that, for the solutions with bare γ^ν, we would have $A(p^2) \equiv 1$ for all values of the coupling. Figure 1(b) shows the masses $M(p^2)$.

Since the equations have no inherent mass scale, the cutoff Λ, renormalization point μ, $m(\mu)$, and units of $M(p^2)$ or $B(p^2)$ all scale multiplicatively, and the units are arbitrary. For instance, the solutions for any given coupling in Fig. 1 could represent a particle with mass 10 MeV at the renormalization point $\mu^2 = -100$ MeV^2, with the units of p^2 in MeV^2 and those of B in MeV; or it could represent one with units in GeV, or in electron masses. Since in four dimensions the coupling has no mass dimension, it would remain unchanged for all such choices of units. This is true for all the graphs that follow.

A comparison of the solutions for the three different vertices, for the coupling $\alpha_0 = 0.5$, is given in Fig. 2. As can be seen in Fig. 2(a), the finite renormalization $A(p^2)$ deviates less from unity in the Curtis-Pennington case. The scalar self-energy curves $B(p^2)$, shown in Fig. 2(b), look qualitatively similar. However, since $M(p^2) = B(p^2)/A(p^2)$, there are differences both in the infrared value of mass (for which we have $M_{\rm CP} < M_{\rm BC} < M_{\rm bare}$ for the same α_0) and in the asymptotic scaling.

The slight difference in scaling of the mass functions for different vertex *Ansätze* is shown in Fig. 3 for $\alpha_0 = 0.5$. Miransky has shown [5] that in Landau gauge with the

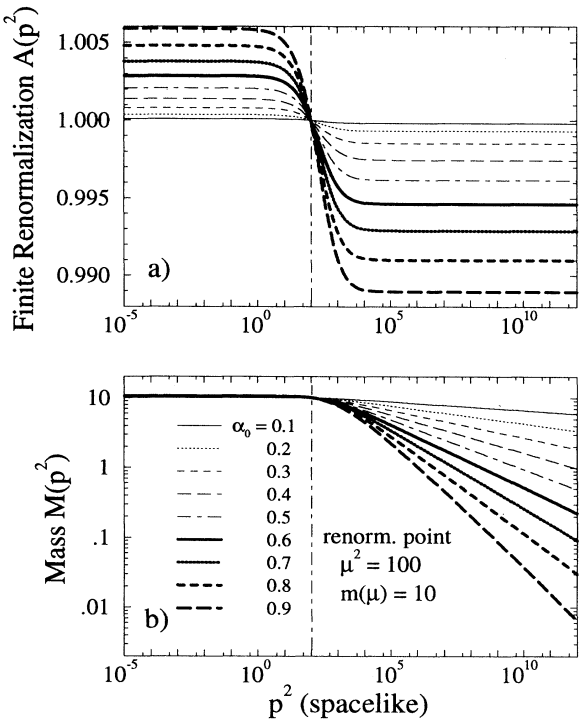

FIG. 1. Family of DSE solutions with the Curtis-Pennington vertex and subcritical couplings $\alpha_0 = 0.1$ to 0.9. The renormalization point is $\mu^2 = 100$, and renormalized mass is $m(\mu) = 10$ for all cases shown. Ultraviolet cutoffs are 1×10^{12} for all cases. (a) the finite renormalizations $A(p^2)$; (b) the mass functions $M(p^2)$.

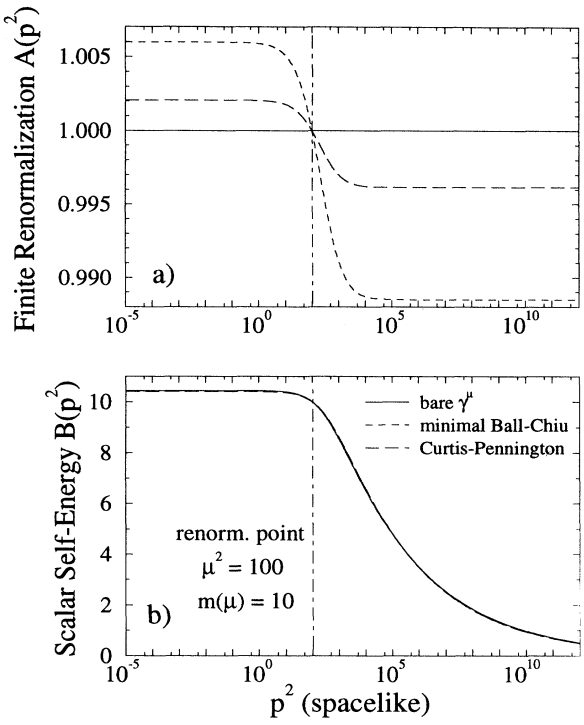

FIG. 2. Comparison of the solutions to the DSE with the three different vertices. All solutions have the subcritical coupling $\alpha_0 = 0.5$, renormalization point $\mu^2 = 100$, and renormalized mass $m(\mu) = 10$. Ultraviolet cutoffs are 1×10^{12} for all cases. (a) the finite renormalizations $A(p^2)$; (b) the scalar self-energy $B(p^2)$.

rainbow approximation, the fermion mass scales asymptotically as $M(p^2) \sim (p^2)^{-(\frac{1}{2}-\gamma')}$ with the anomalous dimension $\gamma'(\alpha_0) = \frac{1}{2}\sqrt{1-\alpha_0/(\pi/3)}$. For $\alpha_0 = 0.5$, the anomalous dimension is $\gamma' = 0.3614329$, giving the power $\frac{1}{2} - \gamma' = 0.138567$. When all the solutions are multiplied by $(p^2)^{\frac{1}{2}-\gamma'(0.5)}$, the difference in anomalous dimensions shows up as a difference in slope of the mass curves on a log-log plot. The anomalous dimensions for the mass functions with Ball-Chiu and Curtis-Pennington vertices are found graphically, to be approximately $\gamma_{BC} = 0.35836$ giving the power $\frac{1}{2} - \gamma_{CP} = 0.14164$, and $\gamma_{CP} = 0.35843$ giving the power $\frac{1}{2} - \gamma_{CP} = 0.14157$, respectively. The small dips apparent at the end of two of these curves are due to having a hard cutoff $\Lambda^2 = 10^{12}$. As Λ is increased these move to higher momenta also.

For the equations with the Curtis-Pennington vertex, the renormalization constants Z_2 and Z_m, and the bare mass $m_0(\Lambda)$ were evaluated for $\alpha_0 = 0.1$ through 0.9, using cutoffs 1×10^{12} and 1×10^{18} and renormalization conditions $\mu^2 = 100$, $m(\mu) = 10$. These are presented in Table I. Specifically for $\alpha_0 = 0.5$, the renormalization constants $Z_2(\mu, \Lambda)$ and $Z_m(\mu, \Lambda)$ were calculated for several values of μ, using cutoffs $\Lambda^2 = 1 \times 10^{12}$ and 1×10^{18}. These are given in Table II, and the mass renormalizations Z_m are plotted as a function of μ^2/Λ^2 in Fig. 4. All these solutions used bare masses chosen so as to dupli-

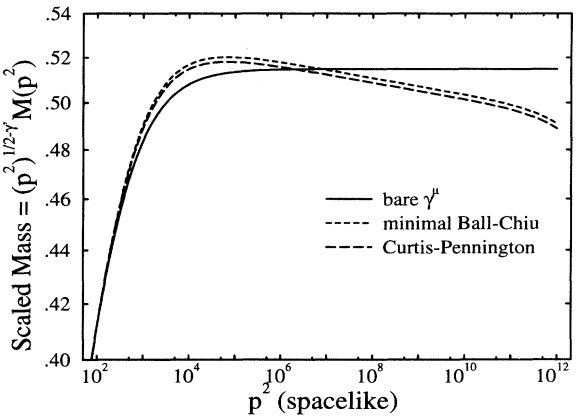

FIG. 3. Asymptotic scaling of the mass function for the three vertex *Ansätze* at the subcritical coupling $\alpha_0 = 0.5$; the functions plotted are $M(p^2) \times (p^2)^{\frac{1}{2}-\gamma'}$, where $\gamma' = 0.3614329$ is the correct anomalous dimension for the bare-vertex solution at this coupling. The anomalous dimensions extracted for the Ball-Chiu and Curtis-Pennington vertices, respectively, are 0.35836 and 0.35843.

TABLE I. Renormalization constants $Z_2(\mu,\Lambda)$, bare masses $m_0(\Lambda)$, and mass renormalization $Z_m(\mu,\Lambda)$ for various subcritical couplings for the Curtis-Pennington vertex, all with $\mu^2 = 100$, $m(\mu) = 10$. Cutoffs Λ^2 are 1×10^{12} and 1×10^{18}.

α_0	Λ^2	$Z_2(\mu,\Lambda)$	$m_0(\Lambda)$	$Z_m(\mu,\Lambda)$
0.1	1×10^{12}	0.99822798	5.74672	0.574672
	1×10^{18}	0.99982280	4.0972	0.40972
0.2	1×10^{12}	0.99931590	3.20125	0.320125
	1×10^{18}	0.99931590	1.59519	0.159519
0.3	1×10^{12}	0.99851308	1.7152	0.17152
	1×10^{18}	0.99851308	0.58245	5.8245×10^{-2}
0.4	1×10^{12}	0.99744429	0.874486	8.74486×10^{-2}
	1×10^{18}	0.99744428	0.195803	1.95803×10^{-2}
0.5	1×10^{12}	0.99613623	0.417692	4.17692×10^{-2}
	1×10^{18}	0.99613623	0.0590025	5.90025×10^{-3}
0.6	1×10^{12}	0.99461286	0.18240	1.8240×10^{-2}
	1×10^{18}	0.99461286	0.015271	1.5271×10^{-3}
0.7	1×10^{12}	0.99289572	0.069783	6.9783×10^{-3}
	1×10^{18}	0.99289572	3.14581×10^{-3}	3.14581×10^{-4}
0.8	1×10^{12}	0.99100430	0.0214029	2.14029×10^{-3}
	1×10^{18}	0.99100429	4.37117×10^{-4}	4.37117×10^{-5}
0.9	1×10^{12}	0.98895625	4.01753×10^{-3}	4.01753×10^{-3}
	1×10^{18}	0.98895626	2.31378×10^{-5}	2.31378×10^{-5}

cate the mass solution for $\mu^2 = 100$, $m(\mu) = 10$. It can be seen that as the value of μ increases, Z_2 approaches 1, and also that Z_2 is almost independent of the cutoff Λ, at least for $\Lambda \gg \mu$. The mass renormalization also scales asymptotically (i.e., for sufficiently large Λ and μ) as $Z_m(\mu,\Lambda) \propto (\mu^2/\Lambda^2)^{\frac{1}{2}-\gamma_{CP}}$. The slight deviation from this scaling behavior evident in Fig. 4 occurs in the region where μ is not sufficiently large.

The solutions are extremely stable as the cutoff is varied. The ultraviolet momentum cutoff is varied by six orders of magnitude with the mass unchanged within numerical accuracy for sufficiently large Λ.

B. Results above the DCSB threshold

The program using the Curtis-Pennington vertex was run with several values of the coupling α_0 from 0.97 to

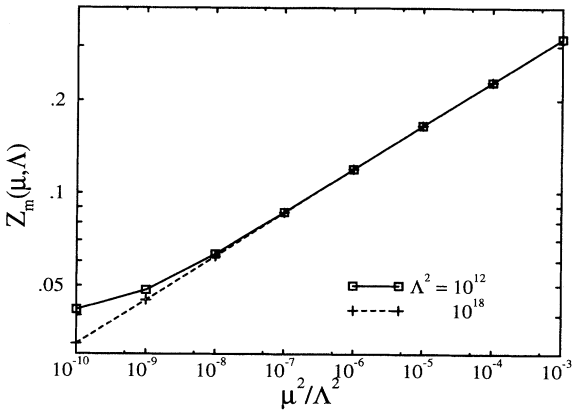

FIG. 4. The mass renormalization Z_m as a function of μ^2/Λ^2, for the subcritical coupling $\alpha_0 = 0.5$. Bare masses for all solutions were chosen to give mass $m(p^2) = 10$ at $p^2 = 100$. Boxes, □, connected by solid lines, are results with cutoff $\Lambda^2 = 1 \times 10^{12}$; pluses, +, connected by dashed lines, are results with $\Lambda^2 = 1 \times 10^{18}$. Data are given in Table II.

1.75, and with several different cutoffs. In all cases the mass and finite renormalization were stable with respect to very large variations in cutoff. Typical results for the self-energy $B(p^2)$ are given in Fig. 5. These were generated using $\alpha_0 = 1.00$, $\mu^2 = 100$, and $m(\mu) = 10$ (in arbitrary units). In both graphs, the cutoff is stepped by factors of 100 over eight orders of magnitude, and again the variation in the solutions is of the order of the tolerance of the calculation.

The bare-vertex DSE was run with couplings $\alpha_0 = 1.15$, 1.5, and 1.75 for comparison to the Curtis-Pennington solutions. A comparison of typical mass curves is given in Fig. 6. Here the mass functions are compared directly since for the bare vertex the scalar self-energy is exactly the mass.

An unexpected feature of the equations (for supercritical couplings only) is that for any set $\{\alpha_0, \mu^2, m(\mu)\}$, as the cutoff is increased there is a small region where the dynamical mass becomes negative. This behavior was verified to be insensitive to the number of grid points, and was stable as the cutoff was increased above the region

TABLE II. Renormalization constants Z_2 and Z_m for several different ratios μ^2/Λ^2; all solutions are for the subcritical coupling $\alpha_0 = 0.5$ for the Curtis-Pennington vertex, with renormalized masses chosen as $m(\mu = 10) = 10$.

	$\Lambda^2 = 1 \times 10^{12}$		$\Lambda^2 = 1 \times 10^{18}$	
μ^2/Λ^2	Z_2	Z_m	Z_2	Z_m
1×10^{-10}	0.99613623	0.04177	0.999999999439219	0.032364
1×10^{-9}	0.99914330	0.04836	0.999999999970789	0.044846
1×10^{-8}	0.99993219	0.06319	0.999999999998478	0.06214
1×10^{-7}	0.99999612	0.08640	0.999999999999921	0.08611
1×10^{-6}	0.99999979	0.11940	0.999999999999995892	0.11932
1×10^{-5}	0.99999998	0.16536	0.999999999999999778	0.16534
1×10^{-4}	0.9999999994	0.22912	1.000000000000000	0.22911
1×10^{-3}	0.99999999997	0.31749		

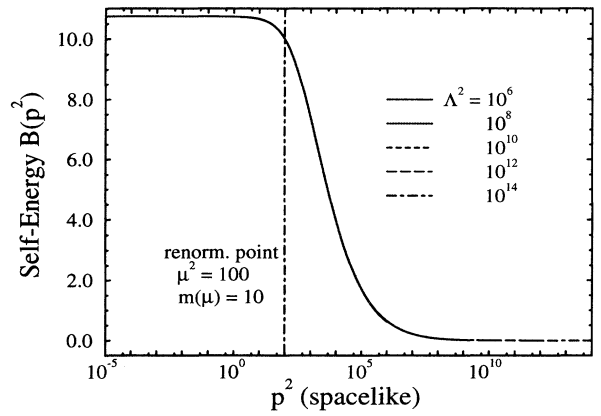

FIG. 5. The scalar self-energy $B(p^2)$, for supercritical coupling $\alpha_0 = 1.00$ for the Curtis-Pennington vertex. Renormalization point is $\mu^2 = 100$, with renormalized mass $m(\mu) = 10$. The cutoff is stepped by factors of 100 over eight orders of magnitude. Note that the mass curves all coincide. Above $p^2 = 2 \times 10^{11}$, the mass curves are negative, but the maximum negative excursion is -2.4×10^{-4}.

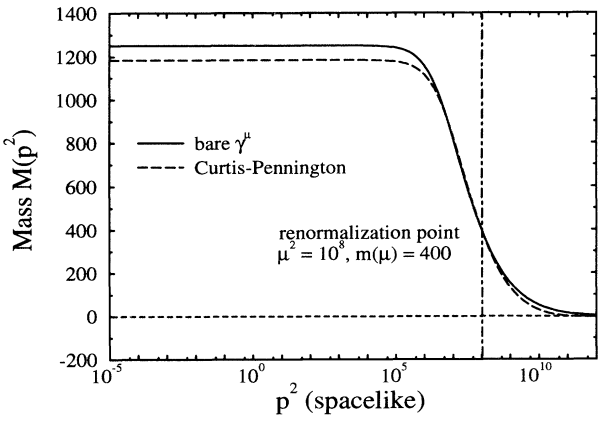

FIG. 6. Mass functions for the supercritical coupling $\alpha_0 = 1.15$ with both the bare and Curtis-Pennington vertices. The renormalization point is $\mu^2 = 1 \times 10^8$, and $m(\mu) = 400$.

TABLE III. Renormalization constants $Z_2(\mu, \Lambda)$, bare masses $m_0(\mu, \Lambda)$, and mass renormalizations $Z_m(\mu, \Lambda)$ for the supercritical coupling $\alpha_0 = 1.15$ for the Curtis-Pennington vertex. All solutions are renormalized with $\mu^2 = 1 \times 10^8$, $m(\mu) = 400$; the cutoff is stepped from 1×10^8 to 1×10^{12}.

Λ^2	μ^2/Λ^2	Z_2	$m_0(\Lambda)$	Z_m
1×10^8	1	0.999913461	230.581	0.57645
1×10^9	0.1	0.999848292	53.5732	0.13393
1×10^{10}	0.01	0.999846784	4.44299	1.1107×10^{-2}
1×10^{11}	0.001	0.999846902	−3.93251	-9.8313×10^{-3}
1×10^{12}	0.0001	0.999846922	−2.84691	-7.1173×10^{-3}

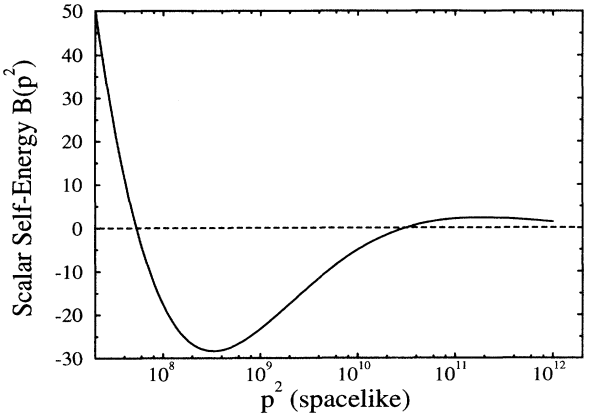

FIG. 7. Zero crossings in the self-energy $B(p^2)$. The case shown has $\alpha_0 = 1.75$, $\mu^2 = 1 \times 10^4$, and $m(\mu) = 500$. Note that there are *two* zero crossings, and that the function approaches zero from above as $p^2 \to \infty$. Note also that the negative peak is typically small compared with $B(0)$, $m(\mu)$, and p^2.

of the negative self-mass, so it seems to be a real effect. The significance of this for QED is not completely understood. One possibility is that it may signal the failure of multiplicative renormalizability for the model DSE, in which case further refinements of the vertex *Ansatz* may be called for. It should be emphasized that this negative dip in the scalar self-energy is very small unless the coupling α_0 approaches 2. For instance, for $\alpha_0 = 1.00$, the negative peak was $\sim 2.4 \times 10^{-5}$ times the size of the renormalized mass. Specifically, we found that for $\mu^2 = 100$, $m(\mu) = 10$, the values are $B(0) = 10.745$, $B(1.634 \times 10^{12}) = -0.00024$; for the case with $\alpha_0 = 1.75$, $\mu^2 = 1 \times 10^4$, $m(\mu) = 500$, the values are $B(0) = 531.8$, $B(3.338 \times 10^8) = -28.3$. An example is shown for $\alpha_0 = 1.75$, $\mu^2 = 1 \times 10^4$, $m(\mu) = 500$ in Fig. 7.

There is no apparent scaling behavior for the mass renormalization Z_m in the supercritical case. The renormalization constant $Z_2(\mu, \Lambda)$ remains finite and well behaved with increasing Λ as expected in the Landau gauge. Typical values, using $\alpha_0 = 1.15$ and the Curtis-Pennington vertex, are given in Table III. From the results in this table and from Eqs. (25,26) we see that $\Sigma_s'(\mu, \Lambda; \mu)$ first increases beyond $m(\mu)$ as Λ increases so that $m_0(\Lambda)$ goes negative. As Λ is further increased the last line of this table indicates that Σ_s' then begins to decrease.

V. SUMMARY AND CONCLUSIONS

We have described preliminary results in a study of four-dimensional quenched QED, with subtractive renormalization performed numerically, during the calculation. We believe that this is the first calculation of its kind, and the technique described here will be applicable elsewhere (e.g., also in QCD), whenever numerical renormalization is required. The importance of this approach

is that it allows studies using different regularization procedures (e.g., various soft versus hard momentum cutoffs) and/or different cutoffs to be meaningfully compared at the same renormalization point. This includes also comparisons with results from lattice studies of QED, which should prove useful in providing further guidance in the choice of reasonable *Ansätze* for the vertex and photon propagator. Without renormalization only the unrenormalized, regulated quantities would be obtained and any such comparisons would be meaningless. In addition, in order to study the nonperturbative behavior of renormalization constants such as $Z_1(\mu,\Lambda)$, $Z_2(\mu,\Lambda)$, and $Z_m(\mu,\Lambda)$ they must be numerically extracted and so a method such as that described here would be essential.

The Curtis-Pennington vertex has been the primary focus of this study, since it has the desirable properties of making the solutions approximately gauge invariant and also multiplicatively renormalizable up to next-to-leading-log order. Solutions have been obtained for comparison purposes, using the minimal Ball-Chiu vertex and using the bare-vertex *Ansätze* (with $Z_1 = Z_2$). For the Ball-Chiu vertex, couplings in the range from $\alpha_0 = 0.1$ to 0.6 were used, while couplings up to $\alpha_0 = 1.75$ were used with both the bare and the Curtis-Pennington vertices. Various renormalization points and renormalized masses were studied.

The subtractive renormalization procedure is straightforward to implement. The solutions are stable and the renormalized quantities become independent of regularization as the regularization is removed, which is as expected. For example, the mass function $M(p^2)$ and momentum-dependent renormalization $Z(p^2)$ are unchanged to within the numerical accuracy of the computation as the integration cutoff is increased by many orders of magnitude. For the range of couplings α_0 considered, the values of the renormalization constant $Z_1(\mu,\Lambda) = Z_2(\mu,\Lambda)$ are never very far from 1 and vary relatively weakly with the choice of renormalized mass and cutoff as expected in Landau gauge. The mass renormalization constant $Z_m(\mu,\Lambda)$ converges with increasing Λ because the mass function $M(p^2)$ falls to zero sufficiently rapidly at large p^2. This is a purely nonperturbative result and is in sharp contrast to the perturbative case where this constant diverges. For subcritical couplings, using the Curtis-Pennington vertex, we also find that the mass renormalization $Z_m(\mu,\Lambda)$ scales approximately as $Z_m(\mu,\Lambda) \propto (\mu^2/\Lambda^2)^{(\frac{1}{2}-\gamma_{\rm CP}(\alpha_0))}$, where, e.g., $\gamma_{\rm CP}(0.5) = 0.358$.

In order to study the critical point and exponents for the transition to DCSB, one would still solve the homogeneous integral equations, i.e., $m(\mu)$ would be chosen to give $m_0(\Lambda) = 0$. The difference between the unrenormalized and renormalized DSE is the multiplication by $Z_2(\mu,\Lambda)$, which can lead to differences in the critical behavior. For example, for the bare vertex with $Z_1 = Z_2 = 1$, we should find the same critical points and exponents as found by Miransky [5]. The critical point for the Curtis-Pennington vertex would remain the same as that found in [26], but the critical exponent would be expected to change due to the variation of Z_2 with α_0.

Extensions of this work to include other gauges, other regularization schemes (e.g., soft cutoffs), studies of the critical behavior, and extraction of the critical exponents, as well as vertices of the Bashir-Pennington type are underway [34].

ACKNOWLEDGMENTS

The authors thank Dr. Craig Roberts for reading the manuscript and for several helpful comments. This work was partially supported by the Australian Research Council, by the U.S. Department of Energy through Contract No. DE-FG05-86ER40273, and by the Florida State University Supercomputer Computations Research Institute which is partially funded by the U.S. Department of Energy through Contract No. DE-FC05-85ER250000. This research was also partly supported by grants of supercomputer time from the U.S. National Energy Research Supercomputer Center and the Australian National University Supercomputer Facility.

[1] K. Johnson, M. Baker, and R. S. Willey, Phys. Rev. **136**, B1111 (1964); **163**, 1699 (1967).
[2] P. I. Fomin, V. P. Gusynin, V. A. Miransky, and Yu. A. Sitenko, Riv. Nuovo Cimento **6**, 1 (1983).
[3] J. E. Mandula, Phys. Lett. **67B**, 175 (1977); A. Hey, D. Horn, and J. E. Mandula, *ibid.* **80B**, 90 (1978); J. Finger, D. Horn, and J. E. Mandula, Phys. Rev. D **20**, 3253 (1979); J. Finger and J. E. Mandula, Nucl. Phys. **B199**, 168 (1982).
[4] P. I. Fomin and V. A. Miransky, Phys. Lett. **64B**, 166 (1976); P. I. Fomin, V. P. Gusynin, and V. A. Miransky, *ibid.* **78B**, 136 (1978); **91B**, 421 (1980).
[5] V. A. Miransky, Sov. Phys. JETP **61** (5), 905 (1985).
[6] V. A. Miransky, Phys. Lett. **165B**, 401 (1985); V. A. Miransky, Nuovo Cimento **90A**, 149 (1985).
[7] A. Cohen and H. Georgi, Nucl. Phys. **B314**, 7 (1989); W. Bardeen, C. N. Leung, and S. T. Love, *ibid.* **B323**, 493 (1989).
[8] U. Mahanta, Phys. Lett. B **225**, 181 (1989).
[9] H. Pagels, Phys. Rev. Lett. **28**, 1482 (1972); T. Maskawa and H. Nakajima, Prog. Theor. Phys. **52**, 1326 (1974); R. Fukuda and T. Kugo, Nucl. Phys. **B117**, 250 (1976).
[10] D. Atkinson and P. W. Johnson, Phys. Rev. D **35**, 1943 (1987); **37**, 2290 (1988).
[11] C. D. Roberts and A. G. Williams, *Dyson-Schwinger Equations and their Application to Hadronic Physics*, in *Progress in Particle and Nuclear Physics, Vol. 33* (Pergamon Press, Oxford, 1994), p. 477.
[12] P. E. L. Rakow, Nucl. Phys. **B356**, 27 (1991).
[13] J. Oliensis and P. W. Johnson, Phys. Rev. D **42**, 656 (1990); K.-I. Kondo and H. Nakatani, Nucl. Phys. **B351**, 236 (1991); K.-I. Kondo, *ibid.* **B351**, 259 (1991).
[14] G. C. Wick, Phys. Rev. **96**, 1124 (1954).
[15] R. Haag and Th. A. Maris, Phys. Rev. **132**, 2325

(1963); Th. A. J. Maris, V. E. Herscovitz, and D. Jacob, Phys. Rev. Lett. **12**, 313 (1964); T. Nonoyama and M. Tanabashi, Prog. Theor. Phys. **81**, 209 (1989).
[16] J. C. Ward, Phys. Rev. **78**, 124 (1950); Y. Takahashi, Nuovo Cimento **6**, 370 (1957).
[17] K.-I. Kondo, Y. Kikukawa, and H. Mino, Phys. Lett. B **220**, 270 (1989).
[18] D. Atkinson, P. W. Johnson, and K. Stam, Phys. Lett. B **201**, 105 (1988).
[19] J. S. Ball and T. W. Chiu, Phys. Rev. D **22**, 2542 (1980); **22**, 2550 (1980).
[20] J. E. King, Phys. Rev. D **27**, 1821 (1983).
[21] P. Rembiesa, Phys. Rev. D **41**, 2009 (1990).
[22] B. Haeri, Phys. Rev. D **43**, 2701 (1991).
[23] D. C. Curtis and M. R. Pennington, Phys. Rev. D **42**, 4165 (1990).
[24] D. C. Curtis and M. R. Pennington, Phys. Rev. D **44**, 536 (1991).
[25] D. C. Curtis and M. R. Pennington, Phys. Rev. D **46**, 2663 (1992).
[26] D. C. Curtis and M. R. Pennington, Phys. Rev. D **48**, 4933 (1993).
[27] Z. Dong, H. Munczek, and C. D. Roberts, Phys. Lett. B **333**, 536 (1994).
[28] A. Bashir and M. R. Pennington, Phys. Rev. D **50**, 7679 (1994).
[29] J. D. Bjorken and S. Drell, *Relativistic Quantum Fields* (McGraw-Hill, New York, 1965).
[30] F. Mandl and G. Shaw, *Quantum Field Theory* (Wiley-Interscience, New York, 1984).
[31] C. D. Roberts, *Schwinger Dyson Equations: Dynamical Chiral Symmetry Breaking and Confinement*, in *QCD Vacuum Structure*, edited by H. M. Fried and B. Müller (World Scientific, Singapore, 1993).
[32] D. Atkinson, J. C. R. Bloch, V. P. Gusynin, M. R. Pennington, and M. Reenders, Phys. Lett. B **329**, 117 (1994).
[33] C. Itzykson and J. B. Zuber, *Quantum Field Theory* (McGraw-Hill, New York, 1980).
[34] F. T. Hawes and A. G. Williams (in preparation).

PHYSICAL REVIEW D VOLUME 51, NUMBER 6 15 MARCH 1995

Chiral symmetry breaking in quenched massive strong-coupling four-dimensional QED

Frederick T. Hawes
Department of Physics and SCRI, Florida State University, Tallahassee, Florida 32306-3016

Anthony G. Williams
Department of Physics and Mathematical Physics, University of Adelaide, South Australia 5005, Australia
(Received 14 October 1994)

We present results from a study of subtractive renormalization of the fermion propagator Dyson-Schwinger equation (DSE) in massive strong-coupling quenched four-dimensional QED. The results are compared for three different fermion-photon proper vertex *Ansätze*: bare γ^μ, minimal Ball-Chiu, and Curtis-Pennington *Ansätze*. The procedure is straightforward to implement and numerically stable. This is the first study in which this technique is used and it should prove useful in future DSE studies, whenever renormalization is required in numerical work.

PACS number(s): 11.30.Rd, 11.30.Qc, 12.20.Ds

I. INTRODUCTION

Strong-coupling QED in three space and one time dimension has been studied within the Dyson-Schwinger equation (DSE) formalism for some time [1–3], in order to see whether there may be a phase transition to a nontrivial "local" theory at high momenta [2,4–6], as a model for dynamical chiral-symmetry-breaking (DCSB) in walking technicolor theories [7,8], and also as an abelianized model for nonperturbative phenomena in QCD [9,10]. For a recent review of Dyson-Schwinger equations and their application see Ref. [11]. The usual approach is to write the DSE for the fermion propagator or self-energy, possibly including equations for the photon vacuum polarization [12,13] or the fermion-photon proper vertex [1]. An *Ansatz* is made for the undefined Green's functions that contain the infinite continuation of the tower of DSE's. The resulting nonlinear integral equations are solved numerically in Euclidean space [14] by iteration. DCSB occurs when the fermion propagator develops a nonzero scalar self-energy in the absence of an explicit chiral-symmetry-breaking (ECSB) fermion mass. We refer to coupling constants strong enough to induce DCSB as supercritical and those weaker are called subcritical. We write the fermion propagator as

$$S(p) = \frac{Z(p^2)}{\not{p} - M(p^2)} = \frac{1}{A(p^2)\,\not{p} - B(p^2)}\ , \qquad (1)$$

with $Z(p^2)$ the finite momentum-dependent fermion renormalization, and $B(p^2)$ the scalar self-energy. In the massless theory (i.e., in the absence of an ECSB bare electron mass) by definition DCSB occurs when $B(p^2) \neq 0$. Note that $A(p^2) \equiv 1/Z(p^2)$ and $M(p^2) \equiv B(p^2)/A(p^2)$.

Many studies, even until quite recently, have used the bare vertex as an *Ansatz* for the one-particle irreducible (1PI) vertex $\Gamma^\nu(k,p)$ [2,4,5,8,9,12,13,15], despite the fact that this violates the Ward-Takahashi identity (WTI) [16]. It is also common, especially in studies motivated by walking technicolor theories [7], to find vertex *Ansätze* which claim to solve the WTI, but which still possess kinematic singularities in the limit of zero photon momentum $q^2 = (k-p)^2 \to 0$ [17,18]. With any of these *Ansätze*, the resulting fermion propagator is not gauge covariant, i.e., physical quantities such as the critical coupling for dynamical symmetry breaking, or the mass itself, are gauge dependent [17]. A general form for $\Gamma^\nu(k,p)$ which does satisfy the Ward identity was given by Ball and Chiu in 1980 [19]; it consists of a minimal longitudinally constrained term which satisfies the WTI, and a set of tensors spanning the subspace transverse to the photon momentum q.

Although the WTI is necessary for gauge invariance, it is not a sufficient condition; further, with many of these vertex *Ansätze* the fermion propagator DSE is not multiplicatively renormalizable, which is equivalent to saying that overlapping logarithms are present. There has been much recent research on the use of the transverse parts of the vertex to ensure both gauge covariant and multiplicatively renormalizable solutions [20–28], some of which will be discussed below.

What is common to essentially all of the studies so far is that the fermion propagator is not in practice subtractively renormalized. Most of these studies have assumed an initially massless theory and have renormalized at the ultraviolet cutoff of the integrations, taking $Z_1 = Z_2 = 1$. Where a nonzero bare mass has been used [6,12], it has simply been added to the scalar term in the propagator. Although there have been formal discussions of the renormalization [5,6,23,26], the important step of subtractive renormalization has not been performed.

We describe here the results of a study of subtractive renormalization in the fermion DSE, in quenched strong-coupling four-dimensional QED (QED_4). (In the context of this study of QED, the term "quenched" means that the bare photon propagator is used in the fermion self-energy DSE, so that $Z_3 = 1$. Virtual fermion loops may still be present, however, within the vertex corrections.) We believe this is the first calculation in which the subtraction is performed numerically as the inte-

gral equations are being iterated. This new technique should prove useful in other DSE studies. Results are obtained for DSE with three different vertices: the bare γ^μ, the minimal Ball-Chiu vertex form [19], and the Curtis-Pennington vertex [23–26].

Organization of the paper is as follows. The DSE for the renormalized fermion propagator, and *Ansätze* for the proper vertex, are discussed in Sec. II. The subtractive renormalization is described in Sec. III. Section IV A presents results at subcritical couplings, while Sec. IV B discusses the results for couplings above the DCSB threshold. Conclusions and discussion are given in Sec. V.

II. DSE AND VERTEX ANSÄTZE

The DSE for the renormalized fermion propagator, in a general covariant gauge, is

$$S^{-1}(p^2) = Z_2(\mu,\Lambda)[\not{p} - m_0(\Lambda)] - iZ_1(\mu,\Lambda)e^2\int^\Lambda \frac{d^4k}{(2\pi)^4}\gamma^\mu S(k)\Gamma^\nu(k,p)D_{\mu\nu}(q)\,; \tag{2}$$

here $q = k - p$ is the photon momentum, μ is the renormalization point, and Λ is a regularizing parameter (taken here to be an ultraviolet momentum cutoff). We write $m_0(\Lambda)$ for the regularization-parameter dependent bare mass. In the massless theory (i.e., in the absence of an ECSB) the bare mass is zero, $m_0(\Lambda) = 0$. The physical charge is e (as opposed to the bare charge e_0), and the general form for the photon propagator is

$$D^{\mu\nu}(q) = \left\{\left(-g^{\mu\nu} + \frac{q^\mu q^\nu}{q^2}\right)\frac{1}{1-\Pi(q^2)} - \xi\frac{q^\mu q^\nu}{q^2}\right\}\,, \tag{3}$$

with ξ the covariant gauge parameter. Since we will work in the quenched approximation and the Landau gauge we have $e^2 \equiv e_0^2 = 4\pi\alpha_0$ and

$$D^{\mu\nu}(q) \to D_0^{\mu\nu}(q) = \left(-g^{\mu\nu} + \frac{q^\mu q^\nu}{q^2}\right)\frac{1}{q^2}\,, \tag{4}$$

for the photon propagator.

A. Vertex Ansatz

The requirement of gauge invariance in QED leads to the Ward-Takahashi identities (WTI); the WTI for the fermion-photon vertex is

$$q_\mu\Gamma^\mu(k,p) = S^{-1}(k) - S^{-1}(p)\,, \tag{5}$$

where $q = k - p$ [29,30]. This is a generalization of the original differential Ward identity, which expresses the effect of inserting a zero-momentum photon vertex into the fermion propagator,

$$\frac{\partial S^{-1}(p)}{\partial p_\nu} = \Gamma^\nu(p,p)\,. \tag{6}$$

In particular, it guarantees the equality of the propagator and vertex renormalization constants, $Z_2 \equiv Z_1$. The Ward-Takahashi identity is easily shown to be satisfied order by order in perturbation theory and can also be derived nonperturbatively.

As discussed in [11,31], this can be thought of as just one of a set of six general requirements on the vertex: (i) the vertex must satisfy the WTI; (ii) it should contain no kinematic singularities; (iii) it should transform under charge conjugation (C), parity inversion (P), and time reversal (T) in the same way as the bare vertex, e.g.,

$$C^{-1}\Gamma_\mu(k,p)C = -\Gamma_\mu^T(-p,-k) \tag{7}$$

(where the superscript T indicates the transpose); (iv) it should reduce to the bare vertex in the weak-coupling limit; (v) it should ensure multiplicative renormalizability of the DSE in Eq. (2); and (vi) the transverse part of the vertex should be specified to ensure gauge covariance of the DSE.

Ball and Chiu [19] have given a description of the most general fermion-photon vertex that satisfies the WTI; it consists of a longitudinally constrained (i.e., "Ball-Chiu") part $\Gamma^\mu_{\rm BC}$, which is a minimal solution of the WTI, and a basis set of eight transverse vectors $T_i^\mu(k,p)$, which span the hyperplane specified by $q_\mu T_i^\mu(k,p) = 0$, $q \equiv k - p$. The minimal longitudinally constrained part of the vertex is given by

$$\Gamma^\mu_{\rm BC}(k,p) = \frac{1}{2}[A(k^2)+A(p^2)]\gamma^\mu + \frac{(k+p)^\mu}{k^2-p^2}\left\{[A(k^2) - A(p^2)]\frac{\not{k}+\not{p}}{2} - [B(k^2)-B(p^2)]\right\}. \tag{8}$$

The transverse tensors are given by

$$T_1^\mu(k,p) = p^\mu(k\cdot q) - k^\mu(p\cdot q)\,, \tag{9}$$
$$T_2^\mu(k,p) = (\not{p}+\not{k})T_1^\mu\,, \tag{10}$$
$$T_3^\mu(k,p) = q^2\gamma^\mu - q^\mu\not{q}\,, \tag{11}$$
$$T_4^\mu(k,p) = p^\nu k^\lambda\sigma_{\nu\lambda}T_1^\mu\,, \tag{12}$$
$$T_5^\mu(k,p) = \sigma^{\mu\nu}q_\nu\,, \tag{13}$$
$$T_6^\mu(k,p) = \gamma^\mu(k^2-p^2) - (k+p)^\mu\not{q}\,, \tag{14}$$
$$T_7^\mu(k,p) = \frac{(k^2-p^2)}{2}[\gamma^\mu(\not{p}+\not{k}) - (k+p)^\mu] + (k+p)^\mu p^\nu k^\lambda\sigma_{\nu\lambda}\,, \tag{15}$$
$$T_8^\mu(k,p) = -\gamma^\mu p^\lambda k^\nu\sigma_{\lambda\nu} - p^\mu\not{k} - k^\mu\not{p}\,. \tag{16}$$

A general vertex is then written as

$$\Gamma^\mu(k,p) = \Gamma^\mu_{\rm BC}(k,p) + \sum_{i=1}^{8} \tau_i(k^2,p^2,q^2) T_i^\mu(k,p) , \quad (17)$$

where the τ_i are functions which must be chosen to give the correct C, P, and T invariance properties.

The work of Curtis and Pennington (CP) [23–26] was mentioned above in connection with the specification of the transverse vertex terms in order to produce gauge invariant and multiplicatively renormalizable solutions to the DSE. In the framework of massless QED_4, they eliminate four of the transverse vectors since they are Dirac even and must generate a scalar term. By requiring that the vertex $\Gamma^\mu(k,p)$ reduce to the leading log result for $k \gg p$ they are led to eliminate all the transverse basis vectors except T_6^μ, with a dynamic coefficient chosen to make the DSE multiplicatively renormalizable. This coefficient has the form

$$\tau_6(k^2,p^2,q^2) = \frac{1}{2}[A(k^2) - A(p^2)]/d(k,p) , \quad (18)$$

where $d(k,p)$ is a symmetric, singularity-free function of k and p, with the limiting behavior $\lim_{k^2 \gg p^2} d(k,p) = k^2$. [Here, $A(p^2) \equiv 1/Z(p^2)$ is their $1/\mathcal{F}(p^2)$.] For purely massless QED, they find a suitable form, $d(k,p) = (k^2 - p^2)^2/(k^2 + p^2)$. This is generalized to the case with a dynamical mass $M(p^2)$, to give

$$d(k,p) = \frac{(k^2-p^2)^2 + [M^2(k^2) + M^2(p^2)]^2}{k^2+p^2} . \quad (19)$$

They establish that multiplicative renormalizability is retained up to next-to-leading-log order in the DCSB case. Subsequent papers establish the form of the solutions for the renormalization and the mass [25] and studied the gauge dependence of the solutions [26]. Dong, Munczek, and Roberts [27] subsequently showed that the lack of exact gauge covariance of the solutions was due to the use of a hard cutoff in the integral equations. The fact that there is still some residual gauge dependence in the physical observables such as the chiral critical point shows that with a hard cutoff the CP vertex *Ansatz* is not yet the ideal choice. Dong, Munczek, and Roberts [27] derived an *Ansatz* for the transverse vertex terms which satisfies the WTI and makes the fermion propagator gauge covariant.

Bashir and Pennington [28] have recently described a vertex *Ansatz* which makes the fermion self-energy exactly gauge covariant, in the sense that the critical point for the chiral phase transition is independent of gauge. Their work is a continuation of that of Dong, Munczek, and Roberts, and indeed their vertex *Ansatz* corresponds to the general form suggested in [27]. However, the kinematic factors $\tau_{2,3,6,8}$ are extremely complicated in form and depend upon a pair of as yet undetermined functions $W_{1,2}(k^2,p^2)$ which must be chosen to guarantee that the weak-coupling limit of Γ^μ matches the perturbative result. Renormalization studies of the DSE using this vertex *Ansatz* should be interesting and represent a direction for further research.

In any case, for the solutions to the fermion DSE using the CP vertex, the critical point for the chiral phase transition has been shown to have a much weaker gauge dependence than that for the DSE with the bare or minimal Ball-Chiu vertices [32]. In this work we will primarily use the Curtis-Pennington *Ansatz* but for the sake of comparison will also present results for the bare vertex. Some solutions are also obtained with the minimal Ball-Chiu vertex which, like the Curtis-Pennington vertex, satisfies the WTI, but which does not lead to approximately gauge-invariant solutions nor multiplicative renormalizability.

For each vertex *Ansatz*, the equations are separated into a Dirac-odd part describing the finite propagator renormalization $A(p^2)$, and a Dirac-even part for the scalar self-energy, by taking $\frac{1}{4}$Tr of the DSE multiplied by $\not{p}/p^2$ and 1, respectively. The equations are solved in Euclidean space and so the volume integrals $\int d^4k$ can be separated into angle integrals and an integral $\int dk^2$; the angle integrations are easy to perform analytically, yielding the two equations which will be solved numerically.

III. THE SUBTRACTIVE RENORMALIZATION

The subtractive renormalization of the fermion propagator DSE proceeds similarly to the one-loop renormalization of the propagator in QED. (This is discussed in [11] and in [33], p. 425ff.) One first determines a finite, *regularized* self-energy, which depends on both a regularization parameter and the renormalization point; then one performs a subtraction at the renormalization point, in order to define the renormalization parameters Z_1, Z_2, Z_3 which give the full (renormalized) theory in terms of the regularized calculation.

A review of the literature of DSEs in QED shows, however, that this step is actually never performed. Curtis and Pennington [26], for example, define their renormalization point at the UV cutoff. Miransky [5] gives a formal discussion of the variation of the mass renormalization $Z_m(\mu,\Lambda)$, but does not implement it numerically.

Many studies take $Z_1 = Z_2 = 1$ [20,22–26]; this is a reasonable approximation in cases where the coupling α_0 is small (i.e., $\alpha_0 \lesssim 1.15$), but if α_0 is chosen large enough, the value of the dynamical mass at the renormalization point may be significantly large compared with its maximum in the infrared. For instance, in [26], figures for the fermion mass are given with $\alpha_0 = 0.97$, 1.00, 1.15, and 2.00 in various gauges. For $\alpha_0 = 2.00$, the fermion mass at the cutoff is down by only an order of magnitude from its limiting value in the infrared.

Repeating the arguments from [11], one defines a regularized self-energy $\Sigma'(\mu,\Lambda;p)$, leading to the DSE for the renormalized fermion propagator:

$$\begin{aligned}\widetilde{S}^{-1}(p) &= Z_2(\mu,\Lambda)[\not{p} - m_0(\Lambda)] - \Sigma'(\mu,\Lambda;p) \\ &= \not{p} - m(\mu) - \widetilde{\Sigma}(\mu;p) , \end{aligned} \quad (20)$$

where the (regularized) self-energy is

$$\Sigma'(\mu,\Lambda;p) = iZ_1(\mu,\Lambda)e^2 \int^{\Lambda} \frac{d^4k}{(2\pi)^4}\gamma^\lambda \widetilde{S}(\mu;k)\widetilde{\Gamma}^\nu(\mu;k,p)\widetilde{D}_{\lambda\nu}(\mu;(p-k)) \,. \tag{21}$$

[To avoid confusion we will follow Ref. [11] and in this section *only* we will denote regularized quantities with a prime and renormalized ones with a tilde, e.g., $\Sigma'(\mu,\Lambda;p)$ is the regularized self-energy depending on both the renormalization point μ and regularization parameter Λ and $\widetilde{\Sigma}(\mu;p)$ is the renormalized self-energy.] As suggested by the notation (i.e., the omission of the Λ dependence) renormalized quantities must become independent of the regularization parameter as the regularization is removed (i.e., as $\Lambda \to \infty$). The self-energies are decomposed into Dirac and scalar parts:

$$\Sigma'(\mu,\Lambda;p) = \Sigma'_d(\mu,\Lambda;p^2)\ \not{p} + \Sigma'_s(\mu,\Lambda;p^2)$$

[and similarly for the renormalized quantity, $\widetilde{\Sigma}(\mu,p)$]. By imposing the renormalization boundary condition

$$\widetilde{S}^{-1}(p)\Big|_{p^2=\mu^2} = \not{p} - m(\mu) \,, \tag{22}$$

one gets the relations

$$\widetilde{\Sigma}_{d,s}(\mu;p^2) = \Sigma'_{d,s}(\mu,\Lambda;p^2) - \Sigma'_{d,s}(\mu,\Lambda;\mu^2) \tag{23}$$

for the self-energy,

$$Z_2(\mu,\Lambda) = 1 + \Sigma'_d(\mu,\Lambda;\mu^2) \tag{24}$$

for the renormalization, and

$$m_0(\Lambda) = \left[m(\mu) - \Sigma'_s(\mu,\Lambda;\mu^2)\right]/Z_2(\mu,\Lambda) \tag{25}$$

for the bare mass. In order to reproduce the case with no ECSB mass, for a given cutoff Λ, one chooses $m(\mu) = \Sigma'_s(\mu,\Lambda;\mu^2)$ so that the bare mass $m_0(\Lambda)$ is zero. The mass renormalization constant is given by

$$Z_m(\mu,\Lambda) = m_0(\Lambda)/m(\mu) \,, \tag{26}$$

i.e., as the ratio of the bare to the renormalized mass.

The vertex renormalization $Z_1(\mu,\Lambda)$ is identical to $Z_2(\mu,\Lambda)$ as long as the vertex *Ansatz* satisfies the Ward identity; this is how it is recovered for multiplication into $\Sigma'(\mu,\Lambda;p)$ in Eq. (21). It will be noticed that this is inappropriate for the bare-vertex *Ansatz* since it fails to satisfy the WTI; nonetheless, since for the bare-vertex case there is no way to determine $Z_1(\mu,\Lambda)$ independently, we will use $Z_1 = Z_2$ for the sake of comparison. In the Landau gauge for the bare vertex these will then both be 1, since in this case $\Sigma'_d(\mu,\Lambda;p^2) = 0$ for all p^2 as is well known [11].

We carry out this step of the renormalization, using the bare vertex γ^μ, the minimal Ball-Chiu vertex of Eq. (8), and that with the Curtis-Pennington transverse term added [see Eqs. (18,19)]. The equations are again first written in Minkowski space, and then rotated to Euclidean space. These are then solved by iteration from an initial guess, with a wide range of cutoffs, and with various renormalization points μ^2 and renormalized masses $m(\mu)$.

IV. RESULTS

Solutions were obtained for the DSE with the Curtis-Pennington and bare vertices, for couplings α_0 from 0.1 to 1.75; solutions were also obtained for the minimal Ball-Chiu vertex, with couplings α_0 from 0.1 to 0.6 (for larger couplings, the DSE with this vertex was susceptible to numerical noise). In Landau gauge, the critical coupling for the DSE with bare vertex is $\alpha_c^{\rm bare} = \pi/3$, the critical coupling for the Curtis-Pennington vertex is $\alpha_c^{\rm CP} = 0.933667$ [32], and that for the Ball-Chiu vertex is expected to be close to these two values. Since there are some qualitative differences between the solutions with subcritical and supercritical couplings, we shall describe these separately.

A. Subcritical couplings

Solutions for the Curtis-Pennington and bare vertex *Ansätze* were obtained for values of the coupling α_0 from 0.1 to 0.9. The program using the Ball-Chiu vertex was also run, with couplings α_0 from 0.1 to 0.6. For the solutions in the subcritical range, the renormalization point $\mu^2 = 100$, and renormalized masses were either $m(\mu) = 10$ or 30. Ultraviolet cutoffs were 1.0×10^{12} and 1.0×10^{18}.

The family of solutions for the Curtis-Pennington vertex with $m(\mu) = 10$ is shown in Fig. 1. Figure 1(a) shows the finite renormalization $A(p^2)$; note that, for the solutions with bare γ^ν, we would have $A(p^2) \equiv 1$ for all values of the coupling. Figure 1(b) shows the masses $M(p^2)$.

Since the equations have no inherent mass scale, the cutoff Λ, renormalization point μ, $m(\mu)$, and units of $M(p^2)$ or $B(p^2)$ all scale multiplicatively, and the units are arbitrary. For instance, the solutions for any given coupling in Fig. 1 could represent a particle with mass 10 MeV at the renormalization point $\mu^2 = -100$ MeV^2, with the units of p^2 in MeV^2 and those of B in MeV; or it could represent one with units in GeV, or in electron masses. Since in four dimensions the coupling has no mass dimension, it would remain unchanged for all such choices of units. This is true for all the graphs that follow.

A comparison of the solutions for the three different vertices, for the coupling $\alpha_0 = 0.5$, is given in Fig. 2. As can be seen in Fig. 2(a), the finite renormalization $A(p^2)$ deviates less from unity in the Curtis-Pennington case. The scalar self-energy curves $B(p^2)$, shown in Fig. 2(b), look qualitatively similar. However, since $M(p^2) = B(p^2)/A(p^2)$, there are differences both in the infrared value of mass (for which we have $M_{\rm CP} < M_{\rm BC} < M_{\rm bare}$ for the same α_0) and in the asymptotic scaling.

The slight difference in scaling of the mass functions for different vertex *Ansätze* is shown in Fig. 3 for $\alpha_0 = 0.5$. Miransky has shown [5] that in Landau gauge with the

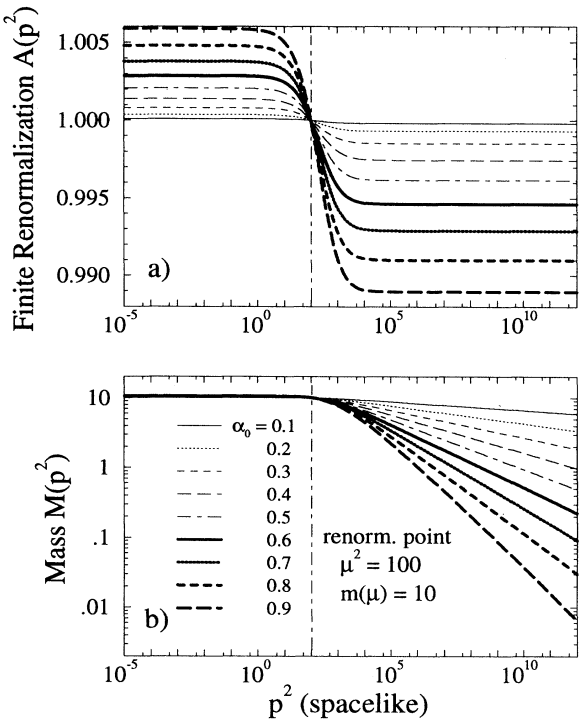

FIG. 1. Family of DSE solutions with the Curtis-Pennington vertex and subcritical couplings $\alpha_0 = 0.1$ to 0.9. The renormalization point is $\mu^2 = 100$, and renormalized mass is $m(\mu) = 10$ for all cases shown. Ultraviolet cutoffs are 1×10^{12} for all cases. (a) the finite renormalizations $A(p^2)$; (b) the mass functions $M(p^2)$.

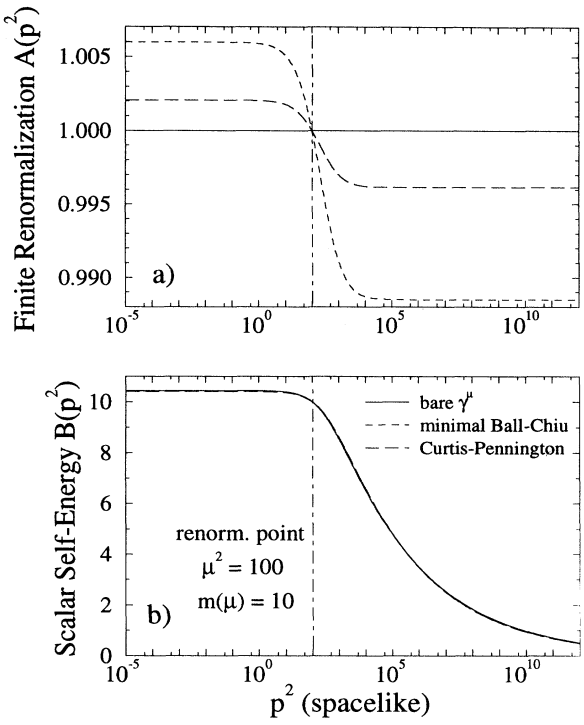

FIG. 2. Comparison of the solutions to the DSE with the three different vertices. All solutions have the subcritical coupling $\alpha_0 = 0.5$, renormalization point $\mu^2 = 100$, and renormalized mass $m(\mu) = 10$. Ultraviolet cutoffs are 1×10^{12} for all cases. (a) the finite renormalizations $A(p^2)$; (b) the scalar self-energy $B(p^2)$.

rainbow approximation, the fermion mass scales asymptotically as $M(p^2) \sim (p^2)^{-(\frac{1}{2}-\gamma')}$ with the anomalous dimension $\gamma'(\alpha_0) = \frac{1}{2}\sqrt{1-\alpha_0/(\pi/3)}$. For $\alpha_0 = 0.5$, the anomalous dimension is $\gamma' = 0.3614329$, giving the power $\frac{1}{2} - \gamma' = 0.138567$. When all the solutions are multiplied by $(p^2)^{\frac{1}{2}-\gamma'(0.5)}$, the difference in anomalous dimensions shows up as a difference in slope of the mass curves on a log-log plot. The anomalous dimensions for the mass functions with Ball-Chiu and Curtis-Pennington vertices are found graphically, to be approximately $\gamma_{BC} = 0.35836$ giving the power $\frac{1}{2} - \gamma_{CP} = 0.14164$, and $\gamma_{CP} = 0.35843$ giving the power $\frac{1}{2} - \gamma_{CP} = 0.14157$, respectively. The small dips apparent at the end of two of these curves are due to having a hard cutoff $\Lambda^2 = 10^{12}$. As Λ is increased these move to higher momenta also.

For the equations with the Curtis-Pennington vertex, the renormalization constants Z_2 and Z_m, and the bare mass $m_0(\Lambda)$ were evaluated for $\alpha_0 = 0.1$ through 0.9, using cutoffs 1×10^{12} and 1×10^{18} and renormalization conditions $\mu^2 = 100$, $m(\mu) = 10$. These are presented in Table I. Specifically for $\alpha_0 = 0.5$, the renormalization constants $Z_2(\mu, \Lambda)$ and $Z_m(\mu, \Lambda)$ were calculated for several values of μ, using cutoffs $\Lambda^2 = 1 \times 10^{12}$ and 1×10^{18}. These are given in Table II, and the mass renormalizations Z_m are plotted as a function of μ^2/Λ^2 in Fig. 4. All these solutions used bare masses chosen so as to dupli-

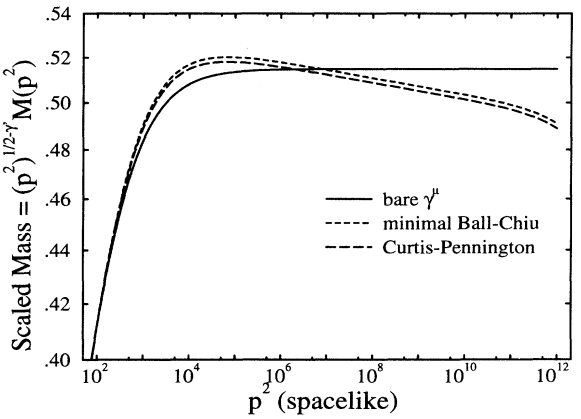

FIG. 3. Asymptotic scaling of the mass function for the three vertex *Ansätze* at the subcritical coupling $\alpha_0 = 0.5$; the functions plotted are $M(p^2) \times (p^2)^{\frac{1}{2}-\gamma'}$, where $\gamma' = 0.3614329$ is the correct anomalous dimension for the bare-vertex solution at this coupling. The anomalous dimensions extracted for the Ball-Chiu and Curtis-Pennington vertices, respectively, are 0.35836 and 0.35843.

TABLE I. Renormalization constants $Z_2(\mu,\Lambda)$, bare masses $m_0(\Lambda)$, and mass renormalization $Z_m(\mu,\Lambda)$ for various subcritical couplings for the Curtis-Pennington vertex, all with $\mu^2 = 100$, $m(\mu) = 10$. Cutoffs Λ^2 are 1×10^{12} and 1×10^{18}.

α_0	Λ^2	$Z_2(\mu,\Lambda)$	$m_0(\Lambda)$	$Z_m(\mu,\Lambda)$
0.1	1×10^{12}	0.99822798	5.74672	0.574672
	1×10^{18}	0.99982280	4.0972	0.40972
0.2	1×10^{12}	0.99931590	3.20125	0.320125
	1×10^{18}	0.99931590	1.59519	0.159519
0.3	1×10^{12}	0.99851308	1.7152	0.17152
	1×10^{18}	0.99851308	0.58245	5.8245×10^{-2}
0.4	1×10^{12}	0.99744429	0.874486	8.74486×10^{-2}
	1×10^{18}	0.99744428	0.195803	1.95803×10^{-2}
0.5	1×10^{12}	0.99613623	0.417692	4.17692×10^{-2}
	1×10^{18}	0.99613623	0.0590025	5.90025×10^{-3}
0.6	1×10^{12}	0.99461286	0.18240	1.8240×10^{-2}
	1×10^{18}	0.99461286	0.015271	1.5271×10^{-3}
0.7	1×10^{12}	0.99289572	0.069783	6.9783×10^{-3}
	1×10^{18}	0.99289572	3.14581×10^{-3}	3.14581×10^{-4}
0.8	1×10^{12}	0.99100430	0.0214029	2.14029×10^{-3}
	1×10^{18}	0.99100429	4.37117×10^{-4}	4.37117×10^{-5}
0.9	1×10^{12}	0.98895625	4.01753×10^{-3}	4.01753×10^{-3}
	1×10^{18}	0.98895626	2.31378×10^{-5}	2.31378×10^{-5}

cate the mass solution for $\mu^2 = 100$, $m(\mu) = 10$. It can be seen that as the value of μ increases, Z_2 approaches 1, and also that Z_2 is almost independent of the cutoff Λ, at least for $\Lambda \gg \mu$. The mass renormalization also scales asymptotically (i.e., for sufficiently large Λ and μ) as $Z_m(\mu,\Lambda) \propto (\mu^2/\Lambda^2)^{\frac{1}{2}-\gamma_{CP}}$. The slight deviation from this scaling behavior evident in Fig. 4 occurs in the region where μ is not sufficiently large.

The solutions are extremely stable as the cutoff is varied. The ultraviolet momentum cutoff is varied by six orders of magnitude with the mass unchanged within numerical accuracy for sufficiently large Λ.

B. Results above the DCSB threshold

The program using the Curtis-Pennington vertex was run with several values of the coupling α_0 from 0.97 to

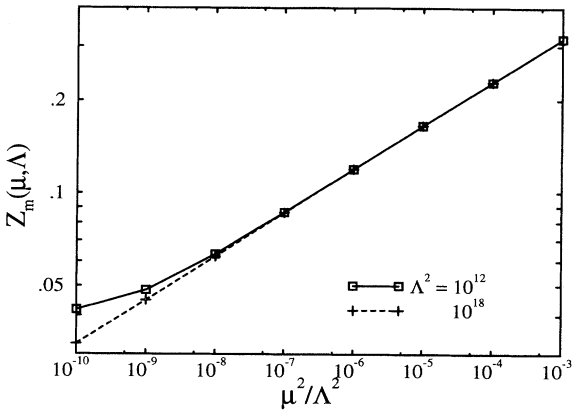

FIG. 4. The mass renormalization Z_m as a function of μ^2/Λ^2, for the subcritical coupling $\alpha_0 = 0.5$. Bare masses for all solutions were chosen to give mass $m(p^2) = 10$ at $p^2 = 100$. Boxes, □, connected by solid lines, are results with cutoff $\Lambda^2 = 1 \times 10^{12}$; pluses, +, connected by dashed lines, are results with $\Lambda^2 = 1 \times 10^{18}$. Data are given in Table II.

1.75, and with several different cutoffs. In all cases the mass and finite renormalization were stable with respect to very large variations in cutoff. Typical results for the self-energy $B(p^2)$ are given in Fig. 5. These were generated using $\alpha_0 = 1.00$, $\mu^2 = 100$, and $m(\mu) = 10$ (in arbitrary units). In both graphs, the cutoff is stepped by factors of 100 over eight orders of magnitude, and again the variation in the solutions is of the order of the tolerance of the calculation.

The bare-vertex DSE was run with couplings $\alpha_0 = 1.15$, 1.5, and 1.75 for comparison to the Curtis-Pennington solutions. A comparison of typical mass curves is given in Fig. 6. Here the mass functions are compared directly since for the bare vertex the scalar self-energy is exactly the mass.

An unexpected feature of the equations (for supercritical couplings only) is that for any set $\{\alpha_0, \mu^2, m(\mu)\}$, as the cutoff is increased there is a small region where the dynamical mass becomes negative. This behavior was verified to be insensitive to the number of grid points, and was stable as the cutoff was increased above the region

TABLE II. Renormalization constants Z_2 and Z_m for several different ratios μ^2/Λ^2; all solutions are for the subcritical coupling $\alpha_0 = 0.5$ for the Curtis-Pennington vertex, with renormalized masses chosen as $m(\mu = 10) = 10$.

	$\Lambda^2 = 1 \times 10^{12}$		$\Lambda^2 = 1 \times 10^{18}$	
μ^2/Λ^2	Z_2	Z_m	Z_2	Z_m
1×10^{-10}	0.99613623	0.04177	0.999999999439219	0.032364
1×10^{-9}	0.99914330	0.04836	0.999999999970789	0.044846
1×10^{-8}	0.99993219	0.06319	0.999999999998478	0.06214
1×10^{-7}	0.99999612	0.08640	0.999999999999921	0.08611
1×10^{-6}	0.99999979	0.11940	0.999999999999995892	0.11932
1×10^{-5}	0.99999998	0.16536	0.999999999999999778	0.16534
1×10^{-4}	0.9999999994	0.22912	1.000000000000000	0.22911
1×10^{-3}	0.99999999997	0.31749		

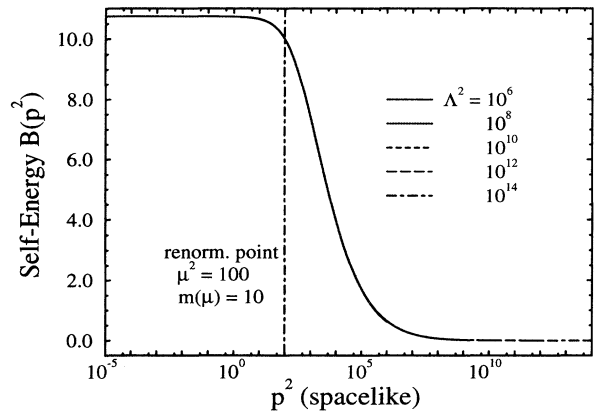

FIG. 5. The scalar self-energy $B(p^2)$, for supercritical coupling $\alpha_0 = 1.00$ for the Curtis-Pennington vertex. Renormalization point is $\mu^2 = 100$, with renormalized mass $m(\mu) = 10$. The cutoff is stepped by factors of 100 over eight orders of magnitude. Note that the mass curves all coincide. Above $p^2 = 2 \times 10^{11}$, the mass curves are negative, but the maximum negative excursion is -2.4×10^{-4}.

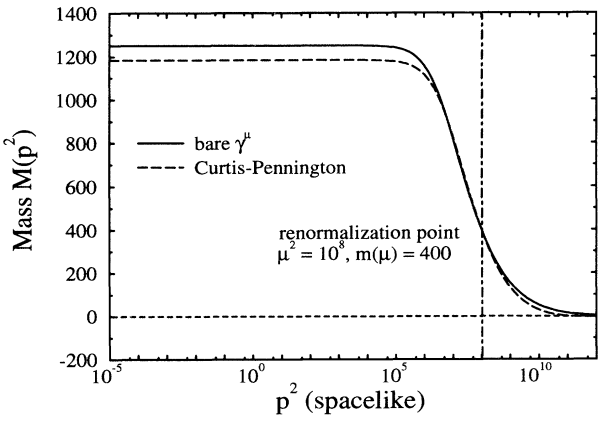

FIG. 6. Mass functions for the supercritical coupling $\alpha_0 = 1.15$ with both the bare and Curtis-Pennington vertices. The renormalization point is $\mu^2 = 1 \times 10^8$, and $m(\mu) = 400$.

TABLE III. Renormalization constants $Z_2(\mu, \Lambda)$, bare masses $m_0(\mu, \Lambda)$, and mass renormalizations $Z_m(\mu, \Lambda)$ for the supercritical coupling $\alpha_0 = 1.15$ for the Curtis-Pennington vertex. All solutions are renormalized with $\mu^2 = 1 \times 10^8$, $m(\mu) = 400$; the cutoff is stepped from 1×10^8 to 1×10^{12}.

Λ^2	μ^2/Λ^2	Z_2	$m_0(\Lambda)$	Z_m
1×10^8	1	0.999913461	230.581	0.57645
1×10^9	0.1	0.999848292	53.5732	0.13393
1×10^{10}	0.01	0.999846784	4.44299	1.1107×10^{-2}
1×10^{11}	0.001	0.999846902	−3.93251	-9.8313×10^{-3}
1×10^{12}	0.0001	0.999846922	−2.84691	-7.1173×10^{-3}

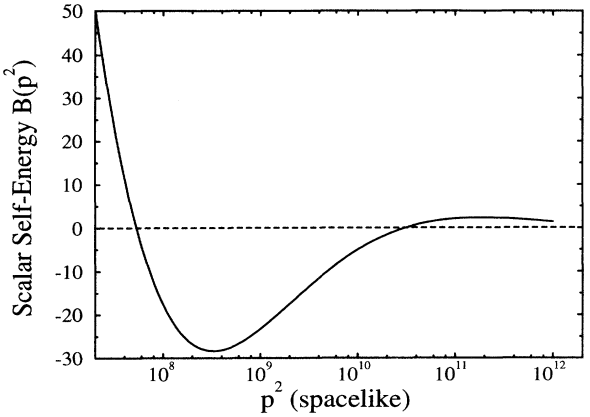

FIG. 7. Zero crossings in the self-energy $B(p^2)$. The case shown has $\alpha_0 = 1.75$, $\mu^2 = 1 \times 10^4$, and $m(\mu) = 500$. Note that there are *two* zero crossings, and that the function approaches zero from above as $p^2 \to \infty$. Note also that the negative peak is typically small compared with $B(0)$, $m(\mu)$, and p^2.

of the negative self-mass, so it seems to be a real effect. The significance of this for QED is not completely understood. One possibility is that it may signal the failure of multiplicative renormalizability for the model DSE, in which case further refinements of the vertex *Ansatz* may be called for. It should be emphasized that this negative dip in the scalar self-energy is very small unless the coupling α_0 approaches 2. For instance, for $\alpha_0 = 1.00$, the negative peak was $\sim 2.4 \times 10^{-5}$ times the size of the renormalized mass. Specifically, we found that for $\mu^2 = 100$, $m(\mu) = 10$, the values are $B(0) = 10.745$, $B(1.634 \times 10^{12}) = -0.00024$; for the case with $\alpha_0 = 1.75$, $\mu^2 = 1 \times 10^4$, $m(\mu) = 500$, the values are $B(0) = 531.8$, $B(3.338 \times 10^8) = -28.3$. An example is shown for $\alpha_0 = 1.75$, $\mu^2 = 1 \times 10^4$, $m(\mu) = 500$ in Fig. 7.

There is no apparent scaling behavior for the mass renormalization Z_m in the supercritical case. The renormalization constant $Z_2(\mu, \Lambda)$ remains finite and well behaved with increasing Λ as expected in the Landau gauge. Typical values, using $\alpha_0 = 1.15$ and the Curtis-Pennington vertex, are given in Table III. From the results in this table and from Eqs. (25,26) we see that $\Sigma_s'(\mu, \Lambda; \mu)$ first increases beyond $m(\mu)$ as Λ increases so that $m_0(\Lambda)$ goes negative. As Λ is further increased the last line of this table indicates that Σ_s' then begins to decrease.

V. SUMMARY AND CONCLUSIONS

We have described preliminary results in a study of four-dimensional quenched QED, with subtractive renormalization performed numerically, during the calculation. We believe that this is the first calculation of its kind, and the technique described here will be applicable elsewhere (e.g., also in QCD), whenever numerical renormalization is required. The importance of this approach

is that it allows studies using different regularization procedures (e.g., various soft versus hard momentum cutoffs) and/or different cutoffs to be meaningfully compared at the same renormalization point. This includes also comparisons with results from lattice studies of QED, which should prove useful in providing further guidance in the choice of reasonable *Ansätze* for the vertex and photon propagator. Without renormalization only the unrenormalized, regulated quantities would be obtained and any such comparisons would be meaningless. In addition, in order to study the nonperturbative behavior of renormalization constants such as $Z_1(\mu,\Lambda)$, $Z_2(\mu,\Lambda)$, and $Z_m(\mu,\Lambda)$ they must be numerically extracted and so a method such as that described here would be essential.

The Curtis-Pennington vertex has been the primary focus of this study, since it has the desirable properties of making the solutions approximately gauge invariant and also multiplicatively renormalizable up to next-to-leading-log order. Solutions have been obtained for comparison purposes, using the minimal Ball-Chiu vertex and using the bare-vertex *Ansätze* (with $Z_1 = Z_2$). For the Ball-Chiu vertex, couplings in the range from $\alpha_0 = 0.1$ to 0.6 were used, while couplings up to $\alpha_0 = 1.75$ were used with both the bare and the Curtis-Pennington vertices. Various renormalization points and renormalized masses were studied.

The subtractive renormalization procedure is straightforward to implement. The solutions are stable and the renormalized quantities become independent of regularization as the regularization is removed, which is as expected. For example, the mass function $M(p^2)$ and momentum-dependent renormalization $Z(p^2)$ are unchanged to within the numerical accuracy of the computation as the integration cutoff is increased by many orders of magnitude. For the range of couplings α_0 considered, the values of the renormalization constant $Z_1(\mu,\Lambda) = Z_2(\mu,\Lambda)$ are never very far from 1 and vary relatively weakly with the choice of renormalized mass and cutoff as expected in Landau gauge. The mass renormalization constant $Z_m(\mu,\Lambda)$ converges with increasing Λ because the mass function $M(p^2)$ falls to zero sufficiently rapidly at large p^2. This is a purely nonperturbative result and is in sharp contrast to the perturbative case where this constant diverges. For subcritical couplings, using the Curtis-Pennington vertex, we also find that the mass renormalization $Z_m(\mu,\Lambda)$ scales approximately as $Z_m(\mu,\Lambda) \propto (\mu^2/\Lambda^2)^{(\frac{1}{2}-\gamma_{\rm CP}(\alpha_0))}$, where, e.g., $\gamma_{\rm CP}(0.5) = 0.358$.

In order to study the critical point and exponents for the transition to DCSB, one would still solve the homogeneous integral equations, i.e., $m(\mu)$ would be chosen to give $m_0(\Lambda) = 0$. The difference between the unrenormalized and renormalized DSE is the multiplication by $Z_2(\mu,\Lambda)$, which can lead to differences in the critical behavior. For example, for the bare vertex with $Z_1 = Z_2 = 1$, we should find the same critical points and exponents as found by Miransky [5]. The critical point for the Curtis-Pennington vertex would remain the same as that found in [26], but the critical exponent would be expected to change due to the variation of Z_2 with α_0.

Extensions of this work to include other gauges, other regularization schemes (e.g., soft cutoffs), studies of the critical behavior, and extraction of the critical exponents, as well as vertices of the Bashir-Pennington type are underway [34].

ACKNOWLEDGMENTS

The authors thank Dr. Craig Roberts for reading the manuscript and for several helpful comments. This work was partially supported by the Australian Research Council, by the U.S. Department of Energy through Contract No. DE-FG05-86ER40273, and by the Florida State University Supercomputer Computations Research Institute which is partially funded by the U.S. Department of Energy through Contract No. DE-FC05-85ER250000. This research was also partly supported by grants of supercomputer time from the U.S. National Energy Research Supercomputer Center and the Australian National University Supercomputer Facility.

[1] K. Johnson, M. Baker, and R. S. Willey, Phys. Rev. **136**, B1111 (1964); **163**, 1699 (1967).
[2] P. I. Fomin, V. P. Gusynin, V. A. Miransky, and Yu. A. Sitenko, Riv. Nuovo Cimento **6**, 1 (1983).
[3] J. E. Mandula, Phys. Lett. **67B**, 175 (1977); A. Hey, D. Horn, and J. E. Mandula, *ibid.* **80B**, 90 (1978); J. Finger, D. Horn, and J. E. Mandula, Phys. Rev. D **20**, 3253 (1979); J. Finger and J. E. Mandula, Nucl. Phys. **B199**, 168 (1982).
[4] P. I. Fomin and V. A. Miransky, Phys. Lett. **64B**, 166 (1976); P. I. Fomin, V. P. Gusynin, and V. A. Miransky, *ibid.* **78B**, 136 (1978); **91B**, 421 (1980).
[5] V. A. Miransky, Sov. Phys. JETP **61** (5), 905 (1985).
[6] V. A. Miransky, Phys. Lett. **165B**, 401 (1985); V. A. Miransky, Nuovo Cimento **90A**, 149 (1985).
[7] A. Cohen and H. Georgi, Nucl. Phys. **B314**, 7 (1989); W. Bardeen, C. N. Leung, and S. T. Love, *ibid.* **B323**, 493 (1989).
[8] U. Mahanta, Phys. Lett. B **225**, 181 (1989).
[9] H. Pagels, Phys. Rev. Lett. **28**, 1482 (1972); T. Maskawa and H. Nakajima, Prog. Theor. Phys. **52**, 1326 (1974); R. Fukuda and T. Kugo, Nucl. Phys. **B117**, 250 (1976).
[10] D. Atkinson and P. W. Johnson, Phys. Rev. D **35**, 1943 (1987); **37**, 2290 (1988).
[11] C. D. Roberts and A. G. Williams, *Dyson-Schwinger Equations and their Application to Hadronic Physics*, in *Progress in Particle and Nuclear Physics, Vol. 33* (Pergamon Press, Oxford, 1994), p. 477.
[12] P. E. L. Rakow, Nucl. Phys. **B356**, 27 (1991).
[13] J. Oliensis and P. W. Johnson, Phys. Rev. D **42**, 656 (1990); K.-I. Kondo and H. Nakatani, Nucl. Phys. **B351**, 236 (1991); K.-I. Kondo, *ibid.* **B351**, 259 (1991).
[14] G. C. Wick, Phys. Rev. **96**, 1124 (1954).
[15] R. Haag and Th. A. Maris, Phys. Rev. **132**, 2325

(1963); Th. A. J. Maris, V. E. Herscovitz, and D. Jacob, Phys. Rev. Lett. **12**, 313 (1964); T. Nonoyama and M. Tanabashi, Prog. Theor. Phys. **81**, 209 (1989).
[16] J. C. Ward, Phys. Rev. **78**, 124 (1950); Y. Takahashi, Nuovo Cimento **6**, 370 (1957).
[17] K.-I. Kondo, Y. Kikukawa, and H. Mino, Phys. Lett. B **220**, 270 (1989).
[18] D. Atkinson, P. W. Johnson, and K. Stam, Phys. Lett. B **201**, 105 (1988).
[19] J. S. Ball and T. W. Chiu, Phys. Rev. D **22**, 2542 (1980); **22**, 2550 (1980).
[20] J. E. King, Phys. Rev. D **27**, 1821 (1983).
[21] P. Rembiesa, Phys. Rev. D **41**, 2009 (1990).
[22] B. Haeri, Phys. Rev. D **43**, 2701 (1991).
[23] D. C. Curtis and M. R. Pennington, Phys. Rev. D **42**, 4165 (1990).
[24] D. C. Curtis and M. R. Pennington, Phys. Rev. D **44**, 536 (1991).
[25] D. C. Curtis and M. R. Pennington, Phys. Rev. D **46**, 2663 (1992).
[26] D. C. Curtis and M. R. Pennington, Phys. Rev. D **48**, 4933 (1993).
[27] Z. Dong, H. Munczek, and C. D. Roberts, Phys. Lett. B **333**, 536 (1994).
[28] A. Bashir and M. R. Pennington, Phys. Rev. D **50**, 7679 (1994).
[29] J. D. Bjorken and S. Drell, *Relativistic Quantum Fields* (McGraw-Hill, New York, 1965).
[30] F. Mandl and G. Shaw, *Quantum Field Theory* (Wiley-Interscience, New York, 1984).
[31] C. D. Roberts, *Schwinger Dyson Equations: Dynamical Chiral Symmetry Breaking and Confinement*, in *QCD Vacuum Structure*, edited by H. M. Fried and B. Müller (World Scientific, Singapore, 1993).
[32] D. Atkinson, J. C. R. Bloch, V. P. Gusynin, M. R. Pennington, and M. Reenders, Phys. Lett. B **329**, 117 (1994).
[33] C. Itzykson and J. B. Zuber, *Quantum Field Theory* (McGraw-Hill, New York, 1980).
[34] F. T. Hawes and A. G. Williams (in preparation).